

Reversible Transition between Thermodynamically Stable Phases with Low Density of Oxygen Vacancies on the SrTiO₃(110) Surface

Fengmiao Li,¹ Zhiming Wang,¹ Sheng Meng,¹ Yongbao Sun,² Jinlong Yang,² Qinlin Guo,¹ and Jiandong Guo^{1,*}

¹Beijing National Laboratory for Condensed-Matter Physics and Institute of Physics, Chinese Academy of Sciences, Beijing 100190, China

²Hefei National Laboratory for Physical Science at the Microscale and University of Science and Technology of China, Hefei, Anhui 230026, China

(Received 8 March 2011; published 14 July 2011)

The surface reconstruction of SrTiO₃(110) is studied with scanning tunneling microscopy and density functional theory (DFT) calculations. The reversible phase transition between (4 × 1) and (5 × 1) is controlled by adjusting the surface metal concentration [Sr] or [Ti]. Resolving the atomic structures of the surface, DFT calculations verify that the phase stability changes upon the chemical potential of Sr or Ti. In particular, the density of oxygen vacancies is low on the thermodynamically stabilized SrTiO₃(110) surface.

DOI: [10.1103/PhysRevLett.107.036103](https://doi.org/10.1103/PhysRevLett.107.036103)

PACS numbers: 68.47.Gh, 31.15.A-, 68.35.Fx, 68.37.Ef

Perovskite oxides have attracted intense interest in the fields of fundamental condensed-matter physics, photocatalysis chemistry, material science, as well as electronics applications, due to their rich phase diagrams and remarkable functionalities. The related research has become even more exciting since the recent discovery of a quasi-two-dimensional electron gas (2DEG) between two insulating materials, SrTiO₃ and LaAlO₃ [1]. Subsequently, a tremendous amount of evidence has shown that the perovskite oxides in the low-dimensional (LD) form such as interfaces, thin films, or heterostructures display an equally rich diversity of exotic phenomena that is related, but not identical, to the bulk [2], indicating a great opportunity for novel oxide-based devices [3]. One of the most important and intriguing discoveries is that the atomic arrangement on the surface or at the interface is determinant for the properties of the entire artificial structure. Hwang *et al.* found that the formation of 2DEG critically depends on the type of atomic termination layer at the interface [1]. Oxygen vacancies (V_O's) also sensitively influence the density and mobility of the charge carriers at the heterointerface of LaAlO₃ and SrTiO₃ [4]. Therefore, to clarify the origin of the emergent properties in LD oxides and ultimately to tune them for the fabrication of functionalized devices, detailed knowledge of their microscopic structures and the high-precision growth technique are the key issues.

Single crystalline SrTiO₃ is widely used as the epitaxial substrate for perovskite oxide films. In order to improve the growth quality, much effort has been made to obtain the atomically flat and ordered SrO or TiO₂ terminated (100) surface [5,6]. In contrast to the electrically neutral (100) surface, the formation process of SrTiO₃(110) surface structure is much more complicated since it is inherently unstable due to the perpendicular macroscopic dipole formed by alternatively stacked (SrTiO)⁴⁺ and (O₂)⁴⁻ layers [7]. The (110) surface stoichiometry often deviates

from that in the ideal crystal, which leads to the formation of mixed phases of reconstruction [8]. V_O's may also be responsible for the stabilization of the (110) surface [9]. Recently Russell *et al.* obtained an (n × 1) (n = 3, 4, 6) family of reconstructions at varying annealing temperatures, which was described as a homologous series with the TiO₄ tetrahedra model [10,11]. However, it is still challenging to understand the stabilization mechanism of SrTiO₃(110) polar surface, particularly the behavior of oxygen (or vacancies).

In this Letter, we investigate the microscopic structure of SrTiO₃(110) surface and present a way of preparing high-quality titanate surfaces and films with ideal oxygen stoichiometry. We obtain the monophased surface in (4 × 1) or (5 × 1) reconstruction. The reversible phase transition between them is realized by tuning Ti or Sr concentration on the surface. With *ab initio* calculations, we determine the atomic structures of both phases and study their stability in different chemical environments. Thus the experimental control of surface reconstruction is understood within the thermodynamic picture. Moreover, both the experimental observations and theoretical calculations reveal that the V_O's density on SrTiO₃(110) surface could be extremely low.

The experiments were performed in an Omicron ultra-high vacuum low temperature scanning tunneling microscopy (STM) system with base pressure of 1 × 10⁻¹⁰ mbar. Nb-doped (0.7 wt %) SrTiO₃(110) single crystals (12 × 3 mm²) were purchased from Hefei KMT Co., China. The as-received sample was sputtered with Ar⁺ beam at room temperature followed by annealing in UHV. Strontium and titanium were evaporated from Knudsen cells, respectively. The flux of Sr was calibrated by observing the formation of Sr/Si(001)-(2 × 1) reconstruction [12] with reflection high-energy electron diffraction (RHEED) and STM, while the flux of Ti was calibrated

by monitoring the RHEED intensity oscillation during the homoepitaxial growth of SrTiO₃(110) film [13]. The sample was resistively heated by passing a direct current and the temperature was monitored with an infrared pyrometer. Density functional theory (DFT) calculations were carried out with the “Vienna *ab initio* simulation package” (VASP) code [14]. We use the projector augmented-wave method [15] and the Perdew–Burke–Ernzerhof functional [16] with the kinetic energy cutoff of 400 eV for plane waves and a $(3 \times 5 \times 1)$ Monkhorst-Pack k -point mesh. The surface structure was modeled with a supercell that was symmetrical along the $[110]$ direction, and consisted of a 13-layer slab separated by a vacuum layer of 12 Å. Atoms in the central three layers were fixed and other atoms were allowed to relax until the force on each atom was less than 0.02 eV/Å. Simulated STM images were generated by integrating the local density of states between Fermi level (E_F) and $E_F + 1.5$ eV in the Tersoff–Hamann approximation [17] with the constant density method [18].

Figure 1(a) shows the monophased (4×1) reconstruction on the SrTiO₃(110) surface after Ar⁺ sputtering (500 eV/2 μA for 10 min) followed by annealing at 1000 °C for 1 h. The surface appears as periodic stripes along the $[1\bar{1}0]$ direction, separated with a dark trench, and each contains two obvious bright rows of periodic dots. The periods along $[1\bar{1}0]$ and $[001]$ are ~ 0.6 and 1.6 nm, respectively, corresponding to the (4×1) reconstruction as observed clearly by RHEED. Evaporating a small amount of Sr metal followed by annealing at 1000 °C, domains with

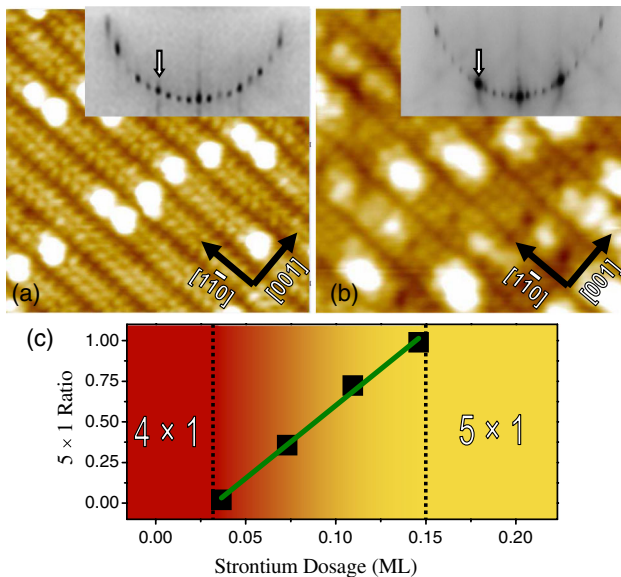


FIG. 1 (color online). (a),(b) STM images (15×15 nm², 1.5 V/20 pA) of (4×1) and (5×1) reconstructed SrTiO₃(110) surfaces, respectively. The insets show the RHEED patterns along $[001]$ direction with (10) spots indicated by arrows, respectively. (c) The area ratio of (5×1) domains through the entire surface depending on the Sr dosage. The statistics are done over 8 STM images (500×500 nm²) for each data point.

a new ordering form on the surface. As shown in Fig. 1(b), it also appears as stripes but wider than that in the (4×1) domain, each containing three bright rows of periodic dots along the $[1\bar{1}0]$ direction. The periods along $[1\bar{1}0]$ and $[001]$ are ~ 0.6 and ~ 1.95 nm, respectively, corresponding to (5×1) reconstruction. The (5×1) domain area enlarges with the Sr evaporation dosage linearly until a monophased surface formed with ~ 0.15 ML Sr [relative to bulk-truncated SrTiO₃(110), 1 ML = 4.64×10^{14} atoms/cm²; see Fig. 1(c)]. Such a phase transition can be reversed by evaporating ~ 0.15 ML Ti onto the (5×1) surface followed by annealing at 1000 °C [13].

With DFT calculations, different structural models of (4×1) reconstruction are compared, including the Sr ad-atom, TiO_x, and (100)-microfaceted models. We find that the TiO₄ tetrahedra model [the left part in Fig. 2(a)] is energetically favorable, consistent with what Enterkin *et al.* reported previously [11]. The simulated STM images reproduce the experimental features very well, as seen in Figs. 2(c) and 2(d). The unoccupied state’s STM image shows both titanium and oxygen atoms on the surface in bright features, as indicated by the ball-and-stick drawing superimposed onto the simulated image. The zigzag TiO₄ chains along $[1\bar{1}0]$ correspond to the bright stripes in the STM images.

Our experimental STM images of the (5×1) reconstruction cannot be described by the $(n \times 1)$ homologous series [11] very well. We modify the initial structure by shifting TiO₄ tetrahedron 1 from the linear chain along $[001]$ to the middle of the zigzag chain along $[1\bar{1}0]$, as

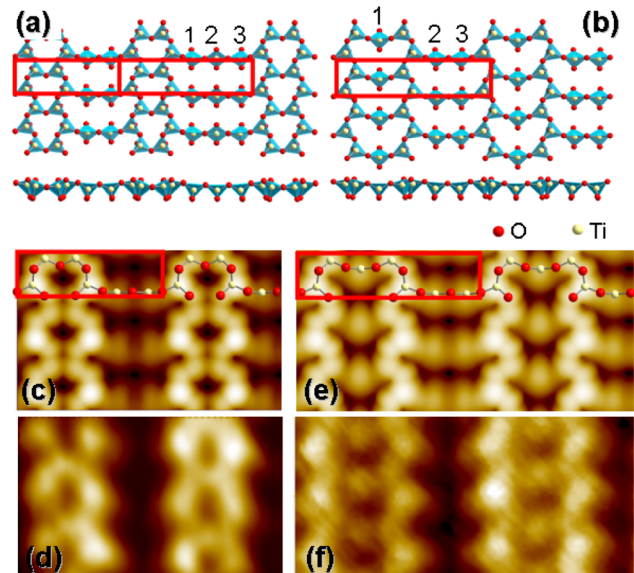


FIG. 2 (color online). (a) The structural model of the $(n \times 1)$ reconstruction [11] with (4×1) on the left and (5×1) on the right. (b) The modified structural model of (5×1) . The upper panels are the top view while the lower panels are the side view. (c),(d) and (e),(f) The simulated and experimental STM images of (4×1) and (5×1) , respectively.

shown in Fig. 2(b) [19]. After relaxation, an extra energy gain of 0.6 eV is obtained comparing with the total energy calculated for the “ $(n \times 1)$ ” model [11]. Although such a small difference could be the result of different functional used in calculations, the simulated image is in excellent agreement with the STM observation on the monophased (5×1) obtained in the current work [Figs. 2(e) and 2(f)].

In the structural models, the nominal area concentration of Ti in (4×1) is higher than that in (5×1) by 0.1 ML. Experimentally, (4×1) or (5×1) phase is formed by increasing the concentration of Ti or Sr, respectively. Quantitatively the evaporation dosage to induce the phase transition (~ 0.15 ML) is higher than the actual difference of the concentration due to a different adhesion coefficient on surfaces of Si(100) (used for calibration) and SrTiO₃(110). In fact, the phase stability strongly depends on the metal concentration on the surface. To further clarify, we calculate the surface free energy of (4×1) and (5×1) phases under different chemical environments, respectively, in terms of chemical potential.

The surface free energy per unit area is defined by

$$\gamma = \frac{1}{2S} [G_{\text{slab}} - N_{\text{Ti}}\mu_{\text{Ti}} - N_{\text{Sr}}\mu_{\text{Sr}} - N_{\text{O}}\mu_{\text{O}}], \quad (1)$$

where G_{slab} is the Gibbs free energy of the slab that can be calculated with our DFT calculations, N is the number of Ti, Sr, or O atoms within the slab, μ is the chemical potential of Ti, Sr, or O, respectively, while S is the area of the symmetrical surface. For the bulk SrTiO₃ crystal, the free energy of each unit cell is

$$G_{\text{SrTiO}_3}^{\text{bulk}} = \mu_{\text{Sr}} + \mu_{\text{Ti}} + 3\mu_{\text{O}}, \quad (2)$$

which equals the energy ($E_{\text{SrTiO}_3}^{\text{bulk}}$) that can be calculated, since the surface is in the thermodynamic equilibrium with the bulk. We use relative chemical potentials $\Delta\mu_{\text{Sr}}$, $\Delta\mu_{\text{Ti}}$, and $\Delta\mu_{\text{O}}$, instead of the chemical potentials, with reference to the energies of a Ti atom in the hcp bulk structure, of a Sr atom in the cubic bulk structure and of an O atom in the O₂ molecule in the gas phase, respectively. And the range of accessible values for them is determined by using the method proposed by Bottin *et al.* [19,20].

Figure 3(a) shows the surface free energy as a function of $\Delta\mu_{\text{Sr}}$ or $\Delta\mu_{\text{Ti}}$ with $\Delta\mu_{\text{O}} = -2$ eV. In a Sr-rich ($\Delta\mu_{\text{Sr}} \rightarrow 0$ eV, or Ti-poor, $\Delta\mu_{\text{Ti}} \rightarrow -9.79$ eV) environment, (5×1) is more stable than (4×1) , while (4×1) is more stable in a Sr-poor (Ti-rich) environment, with the critical concentration $\Delta\mu_{\text{Sr}} = -4.86$ eV, or $\Delta\mu_{\text{Ti}} = -4.93$ eV at $\Delta\mu_{\text{O}} = -2$ eV. The energy difference of the two phases shown in Fig. 3(b) is small. This explains why it has been observed experimentally that the two phases coexist with each other or even with other $(n \times 1)$ phases in fragmentary domains [10].

At different oxygen partial pressure, the phase transition between (4×1) and (5×1) can be induced by the change of Sr or Ti concentration except when $\Delta\mu_{\text{O}}$ is extremely

low, as shown in Figs. 3(c) and 3(d). At our UHV condition, we always observe the (5×1) phase rather than (4×1) when $\Delta\mu_{\text{Sr}}$ is increased by evaporating Sr metal onto the surface. This is in agreement with the calculation even though the phase transition is missing in an ideal O-free environment. However, the calculation predicts that the (5×1) phase should be more stable than (4×1) when $\Delta\mu_{\text{Ti}}$ is high and $\Delta\mu_{\text{O}}$ is low [the labeled zone in Fig. 3(d)], totally in contradiction to the experimental observation that increasing Ti concentration induces the formation of (4×1) phase in UHV. It is suggested that this is experimentally a “forbidden” zone—when the Ti concentration is high, the O concentration cannot be low.

It is not surprising since DFT calculations have revealed that the TiO₄ tetrahedra are energetically stable and normally appear as building blocks of the reconstruction on SrTiO₃ surfaces; i.e., the surface Ti tends to be four-coordinated by oxygen on the thermodynamically stable surface [11]. We calculate the formation energy of V_{O} 's on different layers [19], which illustrates that the energy on the top layer is more than 1 eV higher than on the buried layer. Such a characteristic is similar to that of V_{O} 's on anatase TiO₂(101) surface [21]. In UHV treatment, the main oxygen source is the bulk SrTiO₃. The undercoordinated surface Ti atoms will bind with oxygen atoms diffusing from bulk and form the TiO₄ tetrahedra. Kinetically, oxygen is very diffusive relative to cations in bulk SrTiO₃ [22]. In Figs. 4(a)–4(c), we schematically show how a V_{O} diffuses from the (110) surface towards the bulk. Associated with two three-coordinated Ti atoms, a surface

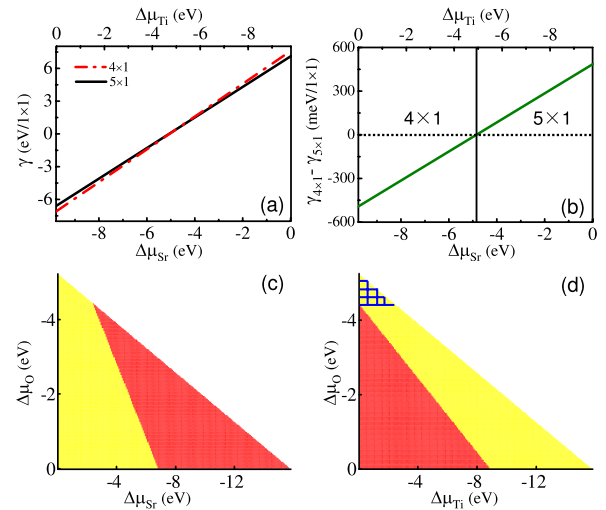


FIG. 3 (color online). (a) The surface free energy of (4×1) (red dashed line) and (5×1) (black solid line) as functions of $\Delta\mu_{\text{Sr}}$ and $\Delta\mu_{\text{Ti}}$, respectively ($\Delta\mu_{\text{O}} = -2$ eV). (b) The energy difference of (4×1) and (5×1) . (c),(d) Phase stability of (4×1) and (5×1) upon Sr and O and Ti and O environments, respectively. The dark gray (red) zones correspond to the environment in which (4×1) is stable while the light gray (yellow) zones correspond to that in which (5×1) is stable.

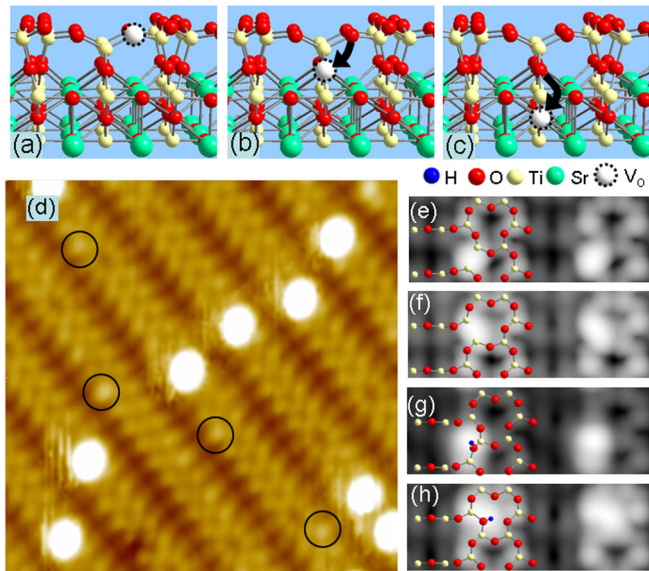


FIG. 4 (color online). (a)–(c) A schematic diagram of the pathway of a V_O diffusing from $\text{SrTiO}_3(110)$ surface towards the bulk. (d) STM image ($10 \times 10 \text{ nm}^2$, 2.0 V) of $\text{SrTiO}_3(110)-(4 \times 1)$. The circles indicate possible V_O 's or hydroxyl-adsorbed V_O 's. (e)–(h) The simulated STM images of (4×1) surface with an oxygen vacancy or a hydroxyl-adsorbed V_O on different sites [19].

V_O is unstable [Fig. 4(a)]. It diffuses to the second layer and then to the fourth layer [Figs. 4(b) and 4(c)]. The energy barrier for both processes is on the order of 0.6 eV as calculated by Cuong *et al.* [23]. Such barriers can be overcome during annealing at 1000°C , and the equilibrium is reached with V_O 's diffusing deep into the bulk.

Comparing with the theoretical simulations [Figs. 4(e)–4(h)], the bright spots labeled with circles in the STM image [Fig. 4(d)] can be attributed to V_O 's or hydroxyl-adsorbed V_O 's (reacted with residual water) on the surface. Statistics of a number of images show that the possible V_O 's density is $\leq 0.4\%$ ML, where 1 ML is defined as the number of oxygen on a perfect (4×1) surface. It is suggested that the thermodynamically stable surface is experimentally reached.

It has been a great challenge to control the V_O 's density or to minimize it to obtain an oxide surface or other LD structures with ideal stoichiometry. Highly reactive oxygen sources are employed at a high partial pressure during the growth with molecule beam epitaxy (MBE) or pulsed-laser deposition technique. However, such a tuning is limited since the growth mode of films changes from two-dimensional layer by layer to three-dimensional island growth when the oxygen pressure exceeds 10^{-2} mbar [24]. Moreover, specifically in MBE, the oxidation of the metal sources is also an important issue. The oxygen properties near the $\text{SrTiO}_3(110)$ surface region suggests a method to epitaxially grow high-quality titanate films

along $[110]$ —as long as the metal stoichiometry is well controlled, V_O 's can be eliminated with low growth rate at high temperature.

In conclusion, we obtain atomically well defined (4×1) and (5×1) reconstructions on $\text{SrTiO}_3(110)$ surface. With *ab initio* calculations we resolve the microscopic structures and explain the phase transition between the two phases in terms of the surface free energy determined by metal concentration. Moreover, the V_O 's density on the reconstructed $\text{SrTiO}_3(110)$ surface could be extremely low, suggesting a feasible way to grow high-quality thin films of perovskite titanates.

The authors are grateful for the discussion with Jiandi Zhang (LSU). This work is supported by NSFC (10704084 and 11074287) and MOSTC (2007CB936800). The calculation results were obtained on the Deepcomp7000 of Supercomputing Center, Computer Network Information Center of Chinese Academy of Sciences.

*jdguo@aphy.iphy.ac.cn

- [1] A. Ohtomo and H. Hwang, *Nature (London)* **427**, 423 (2004).
- [2] For a review, see *J. Phys. Condens. Matter* **20**, 260301 (2008).
- [3] J. Mannhart and D. Schlom, *Science* **327**, 1607 (2010).
- [4] W. Siemons *et al.*, *Phys. Rev. B* **76**, 155111 (2007).
- [5] M. Kawasaki *et al.*, *Science* **266**, 1540 (1994).
- [6] G. Koster *et al.*, *Appl. Phys. Lett.* **73**, 2920 (1998).
- [7] C. Noguera, *J. Phys. Condens. Matter* **12**, R367 (2000).
- [8] J. Brunen and J. Zegenhagen, *Surf. Sci.* **389**, 349 (1997).
- [9] Y. Mukunoki *et al.*, *Appl. Phys. Lett.* **86**, 171908 (2005).
- [10] B. C. Russell and M. R. Castell, *Phys. Rev. B* **77**, 245414 (2008).
- [11] J. A. Enterkin *et al.*, *Nature Mater.* **9**, 245 (2010).
- [12] J. W. Reiner *et al.*, *Phys. Rev. Lett.* **101**, 105503 (2008).
- [13] Z. Wang *et al.*, *Phys. Rev. B* **83**, 155453 (2011).
- [14] G. Kresse and J. Furthmüller, *Phys. Rev. B* **54**, 11 169 (1996); G. Kresse and J. Hafner, *Phys. Rev. B* **47**, R558 (1993).
- [15] P. E. Blöchl, *Phys. Rev. B* **50**, 17953 (1994).
- [16] J. P. Perdew, K. Burke, and M. Ernzerhof, *Phys. Rev. Lett.* **77**, 3865 (1996).
- [17] J. Tersoff and D. R. Hamann, *Phys. Rev. Lett.* **50**, 1998 (1983).
- [18] D. E. P. Vanpoucke and G. Brocks, *Phys. Rev. B* **77**, 241308 (2008).
- [19] See Supplemental Material at <http://link.aps.org/supplemental/10.1103/PhysRevLett.107.036103> for crystallographic information files, structure images, calculations of surface energy and V_O 's formation energy, and STM simulations.
- [20] F. Bottin, F. Finocchi, and C. Noguera, *Phys. Rev. B* **68**, 035418 (2003).
- [21] H. Cheng and A. Selloni, *Phys. Rev. B* **79**, 092101 (2009).
- [22] A. Paladino *et al.*, *J. Phys. Chem. Solids* **26**, 391 (1965).
- [23] D. D. Cuong *et al.*, *Phys. Rev. Lett.* **98**, 115503 (2007).
- [24] M. Huijben *et al.*, *Adv. Mater.* **21**, 1665 (2009).